Int J Adv Manuf Technol (2015) 77:1191–1203
DOI 10.1007/s00170-014-6523-y

ORIGINAL ARTICLE

Influence of complex structure on the shrinkage of part in investment casting process

Changhui Liu · Sun Jin · Xinmin Lai · Bo He · Fei Li

Received: 9 June 2014 / Accepted: 20 October 2014 / Published online: 6 November 2014

Abstract Investment casting (IC) is traditionally used to produce high accuracy products, but the products gaining variable cross section, multidimensional, and unconstrained/constrained features make it hard to determine the tooling dimensions. Every individual stage in the investment casting process (ICP) also poses a potential and uncertain threat on the final part dimensions. In this article, a variable cross section, multidimensional and unconstrained/constrained part for IC, is designed and constructed. The dimensions of wax pattern and final casting part are measured by three-dimensional (3-D) laser scanning, and the inner cavity dimensions of the ceramic shell are measured by industrial computerized tomography (ICT). The dimensional changes and the change of shrinkage along with the dimensions in different processes are analyzed. Finally, the exponential relationship between shrinkage and dimension in the whole ICP is concluded, and the mechanisms of the dimensional changes are discussed. The conclusions can be used to guide the dimensional design of the die and the reworking of the wax pattern to reduce the trial-and-error procedures.

Keywords Shrinkage · Variable cross section · Multidimension · Unconstrained/constrained · Investment casting

C. Liu
Shanghai Key Laboratory of Digital Manufacture for Thin-walled Structures, Shanghai Jiao Tong University, Shanghai 200240, People's Republic of China
e-mail: liuchanghui@sjtu.edu.cn

S. Jin (✉) · X. Lai
State Key Laboratory of Mechanical System and Vibration, Shanghai Jiao Tong University, 800 Dongchuan RD, Minhang District, Shanghai 200240, People's Republic of China
e-mail: jinsun@sjtu.edu.cn

X. Lai
e-mail: xmlai@sjtu.edu.cn

B. He · F. Li
State Key Laboratory of Metal Matrix Composites, Shanghai Jiao Tong University, 800 Dongchuan RD, Minhang District, Shanghai 200240, People's Republic of China

B. He
e-mail: hebo@sjtu.edu.cn

F. Li
e-mail: lifei@sjtu.edu.cn

1 Introduction

Investment casting (IC) is employed to produce parts with intricate geometry and high degree of dimensional accuracy [1, 2]. In order to obtain the final casting parts with accurate dimensions, a reasonable design of the dimensions of pattern die is very difficult to obtain in the investment casting process (ICP). As a multistep process, the ICP consists of the production of wax parts, the production of the ceramic shell, and the metal casting. All of these stages have their own complexities and pose a potential and uncertain threat on the prediction of tooling dimensions.

The influence of the pattern geometry on the dimensions of the final casting part is also significant. It is especially difficult to predict dimensional changes caused by the solidification of wax and metal. Because of the complex geometric features, such as local constrained and local unconstrained, the cooling rates of wax or metal are different, and it results in a nonuniform and complex shrinking of the part [2].

However, with the continuous development of space flight, national defense, and the automobile industry, the products of IC such as blade and casing are gaining variable cross section, multidimensional, and unconstrained/constrained features, and the required precision in the final casting of the geometry

is also growing [3, 4]. All of these make it difficult to determine the dimensions of pattern die.

For unconstrained dimensions (i.e., neither cores nor die pieces limit the shrinking of the part), the tooling predictions are easy, because the dimensions of the final part are only determined by their own thermal expansion property. However, for constrained dimensions, IC engineers just have to rely on trial and error and on their experience to design the shrinkage allowances. The pattern die is often reworked several times so that the dimensions of castings are within acceptable tolerances.

Although three-dimensional (3-D) computer-aided designs (CADs) are used in the casting process widespread [5, 6] and some simulation programs have become increasingly important (i.e., Moldflow, Procast), only limited accuracy can be attained with these software packages, especially for the parts with complex constrained dimensions. Gebelin and Jolly simulated experimental works of different stages in the ICP via different models and highlighted the shortcoming of the accuracy of most commercial software by comparing the experimental and numerical results [7]. Therefore, more attention should be paid to the ability to control and improve the IC accuracy of the parts with complex structure.

To improve the precision of the final casting part with complex structure, a lot of studies have been done in different stages [8, 9]. Studies show that the precision of the final casting part is mainly inherited from its corresponding wax pattern [1, 10–12]. Hock et al. indicated that the contractions of unconstrained wax patterns are more than those of constrained wax patterns in wax injection process [13]. Rahmati et al. pointed out that the constrained dimensions have an average shrinkage of 0.65 %percent, but that of the unconstrained dimensions is 2.85 % [14]. In the report of Morrell et al., the dimensional stability of ceramic shell was investigated via a suite of laboratory tests as well as plant casting trials. The results show that in order to acquire a tight casting tolerance, the role that the accuracy of ceramic shell plays is important [15]. Jiang and Liu considered the influences of restrictions/interactions using a pyramid-shaped part and indicated that not only the dimensional changes but also the dimensional variation of shell were affected soundly by the orientation, location, and dimension of a feature on the part [16]. Based on the thin shell fabrication technology of IC, Jiang et al. proposed a new shell casting process for manufacturing complicated and thin-walled aluminum and magnesium alloy precision castings [17]. In the casting process, a part with six steps and two holes, considering the effects of the different dimensions and unconstrained/constrained structure on the shrinkage of casting was designed and showed that the shrinkage of metal in casting process made a significant contribution to the overall dimensional changes in the whole ICP [18–20]. For the complex and constrained structure, turbine blade attracts a lot of attentions [21–23]. Dong et al. proposed a geometric parameterized model to remedy the blade shrinkages at different positions so that the dimensional accuracy of the turbine blades can be guaranteed [24].

So far, it can be seen that much work has been done in the area of dimensional changes of the parts with complex structures in the ICP and there is significant information in the literature on these processes. However, most studies just focus on the dimensional change of the individual stage, and there has been limited application for the tooling prediction in the ICP. Study of the influence of the pattern geometry on the shrinkage of the whole ICP in more depth is still significative.

In this paper, a ring to ring, variable cross section, multidimensional, and unconstrained/constrained part is designed. The dimensions of wax pattern and final casting part are measured by 3-D laser scanning, the inner cavity dimensions of the ceramic shell are measured by industrial computerized tomography (ICT), and the shrinkages of different thicknesses, external diameters, and inner diameter at every stage are calculated. The characteristic of dimensional changes in the whole ICP is revealed and discussed. Then, the shrinkage of different thicknesses and that of different external diameters is analyzed. Finally, the relationship between the shrinkage and geometrical features is unveiled via the analysis and comparison.

2 Experimental methodology

2.1 Test part design and shrinkage measurements

The structure of the produced test part is shown in Fig. 1. It has dimensions with a maximum external diameter of 348 mm and height of 125 mm. The stepped part thicknesses are 2, 4, 8, 16, and 24 mm. The dimensions of the part are shown in Fig. 2. The considering factors are the following:

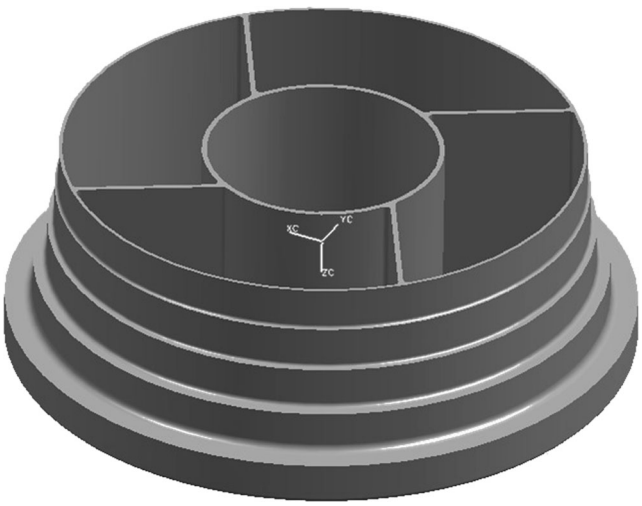

Fig. 1 Structure of the test part

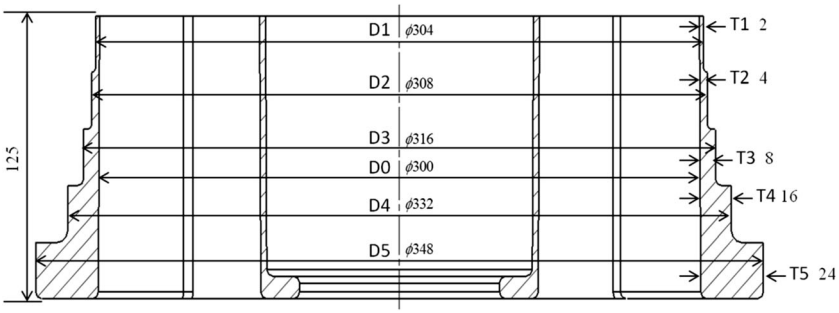

Fig. 2 Dimensions of the test part

1. The part is a ring to ring part with multidiameters to reflect the characteristic of multidimensional feature, and its measurement should be easy. Unconstrained and constrained features should also be included. In this study, the inner diameters are constrained dimensions and the external diameters are unconstrained diameters.
2. The part should reflect the variable cross section of castings. The five steps of the part reflect the variable cross section feature.

In order to get the changes of 3-D dimensions visually, the dimensions of die, wax pattern, and final casting part were measured by means of 3-D laser scanning with ±35-μm accuracy. Using laser measuring system (FARO), the 3-D point cloud model can be obtained. The ICT with ±8-μm accuracy was applied to measure the inner cavity dimensions of the ceramic shell. Importing the processed point cloud data and the theoretical CAD model into Geomagic Qualify [25, 26], by using 3-D comparison function, the errors between the theoretical CAD model and the point cloud data in different stages were compared. The same cross section contour of the part in different stages can also be compared, and the distance between section lines can be calculated and analyzed. Then, the shrinkages of every stage were calculated. In order to guide the dimensional design of the die and the reworking of the wax pattern to ensure correct dimensions and improve the accuracy of the final casting part, the shrinkage from the wax to the final casting part and the total shrinkage were also

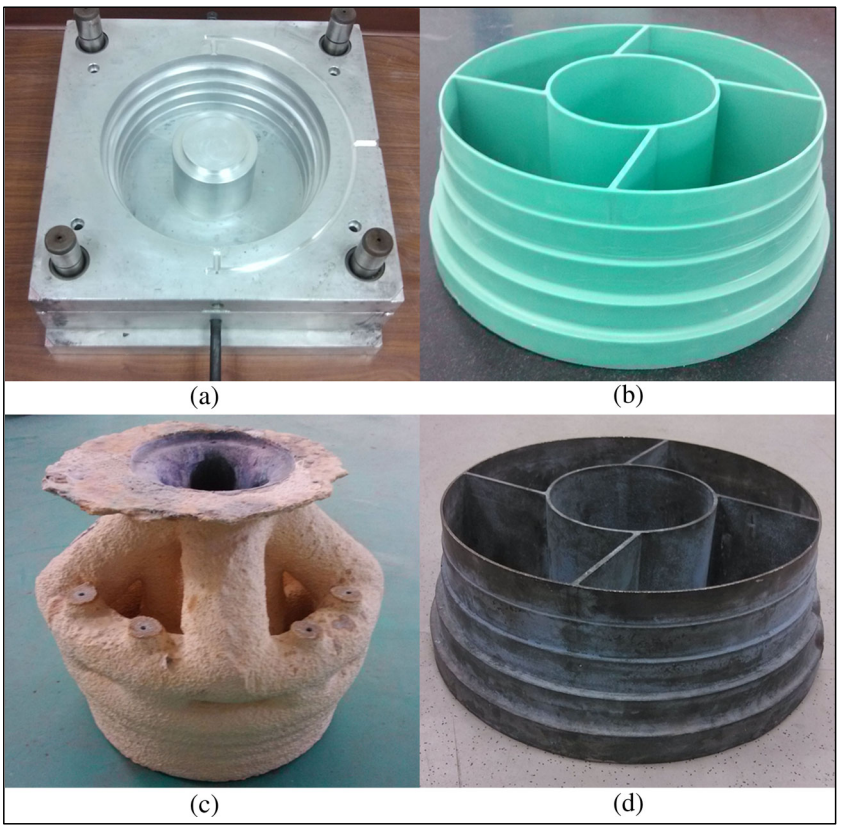

Fig. 3 Part in different stages. **a** Die, **b** wax pattern, **c** ceramic shell after dewaxing, and **d** casting part

Table 1 Process parameters of wax injection

Process parameters	Value
Mold temperature (°C)	25
Melt temperature (°C)	72
Injection velocity (cm^3/s)	125
Holding time (s)	17
Packing pressure (bar)	30
V/P switch-over (volume)	99 %
Clamp force (t)	51.2
Cycling time	35

calculated. These shrinkages can be calculated with the following equations:

$$S_{\text{wax}} = \frac{L_{\text{wax}}}{L_{\text{die}}} \times 100\% \quad (1)$$

$$S_{\text{shell}} = \frac{L_{\text{shell}}}{L_{\text{wax}}} \times 100\% \quad (2)$$

$$S_{\text{casting}} = \frac{L_{\text{casting}}}{L_{\text{shell}}} \times 100\% \quad (3)$$

$$S_{\text{casting-wax}} = \frac{L_{\text{casting}}}{L_{\text{wax}}} \times 100\% \quad (4)$$

$$S_{\text{total}} = \frac{L_{casting}}{L_{\text{die}}} \times 100\% \quad (5)$$

where L_{die}, L_{wax}, L_{shell}, and L_{casting} are the dimensions (diameters and thicknesses are considered in this study) of die, wax pattern, shell, and final casting part, respectively. S_{wax}, S_{shell}, and S_{casting} are the shrinkages of wax in the wax injection, shell in the dewaxing, and casting part in the casting process, respectively. $S_{casting-wax}$ is the shrinkage of final casting part relative to wax pattern, and S_{total} is the shrinkage of the final casting part in the whole ICP.

The final casting relative to the wax pattern and the total shrinkage can also be written as follows:

$$S_{\text{casting-wax}} = S_{\text{shell}}.S_{\text{casting}} \quad (6)$$

$$S_{\text{total}} = S_{\text{wax}}.S_{\text{shell}}.S_{\text{casting}} \quad (7)$$

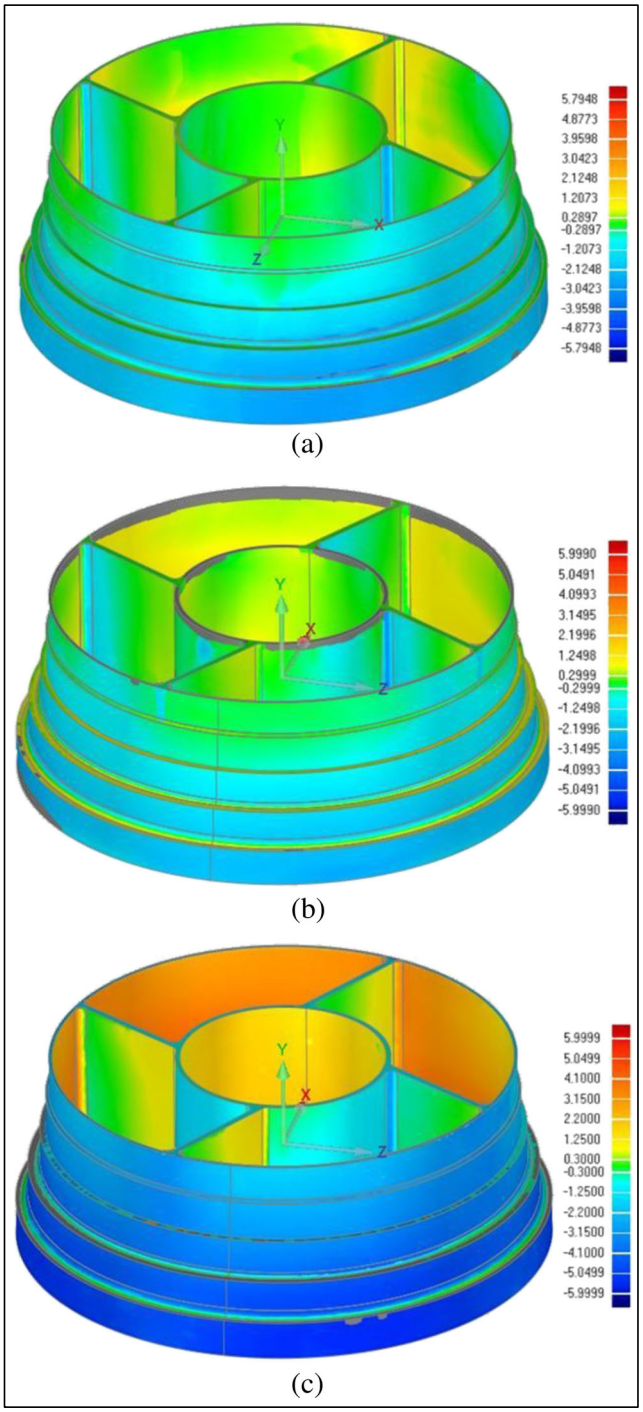

Fig. 4 3-D comparing results of the measured point cloud model relative to the CAD model. **a** Wax, **b** ceramic shell, and **c** casting part

According to this definition of shrinkage, if the shrinkage is greater than 1, that means that the dimension expands and greater shrinkage means more dramatic expansion; a shrinkage less than 1 indicates that the dimension shrinks and the smaller shrinkage indicates more dramatic shrink.

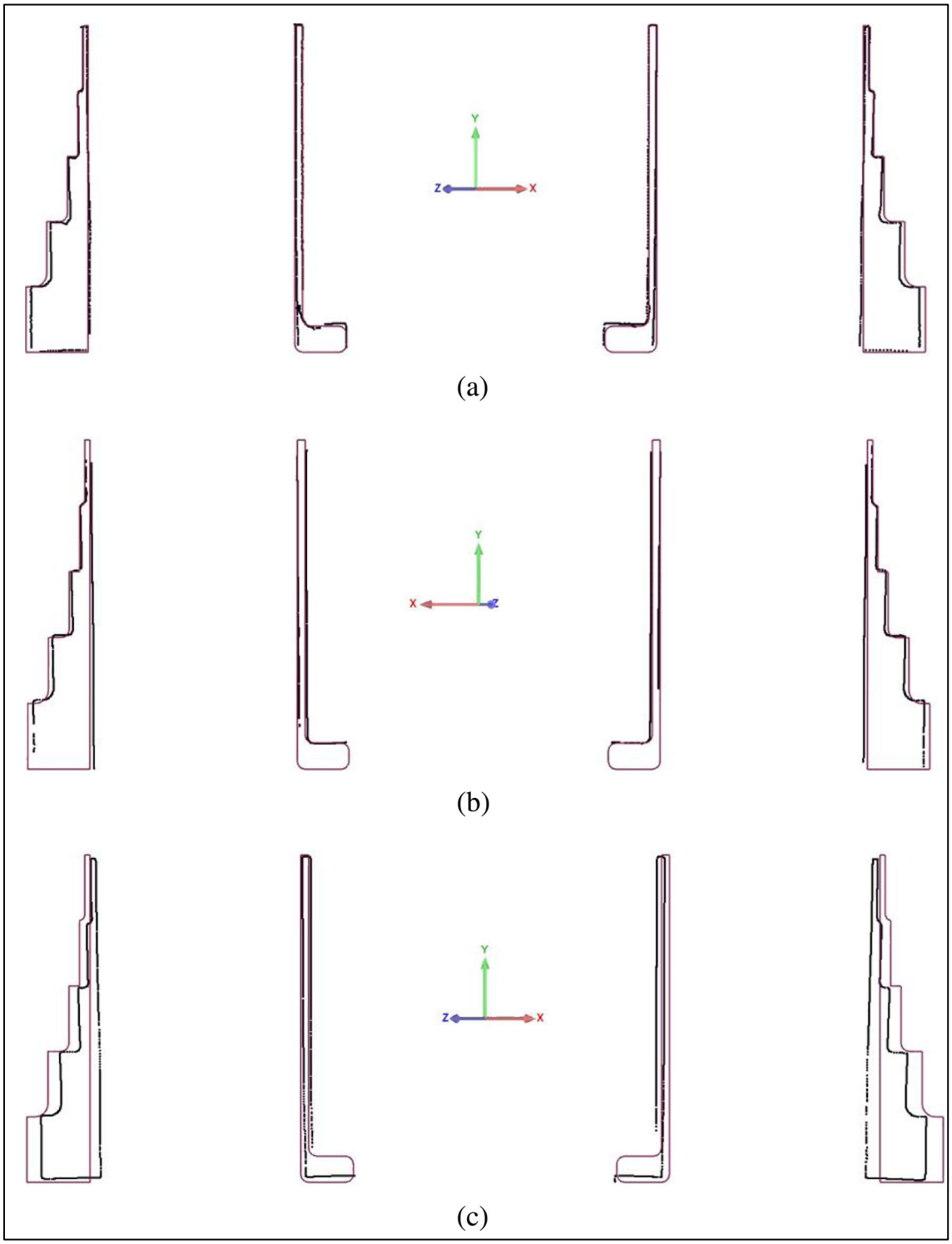

Fig. 5 2-D comparing results of the measured point cloud model relative to the CAD model. **a** Wax, **b** ceramic shell, and **c** casting part

2.2 Creation of test parts

2.2.1 Wax pattern construction and material

The commercial waxes, KC4017B, which were manufactured by Kindt-Collins with a ring and ball softening point of 64.4 °C, were used, and the die was made of aluminum alloy 7075. The wax pattern was constructed by MPI55-100 injection molding machine, with adjusting the experimental parameters via a control program. This wax injection machine has the technical specifications of a maximum clamp force of 100 t, a maximum injection pressure of 70 bar, a maximum

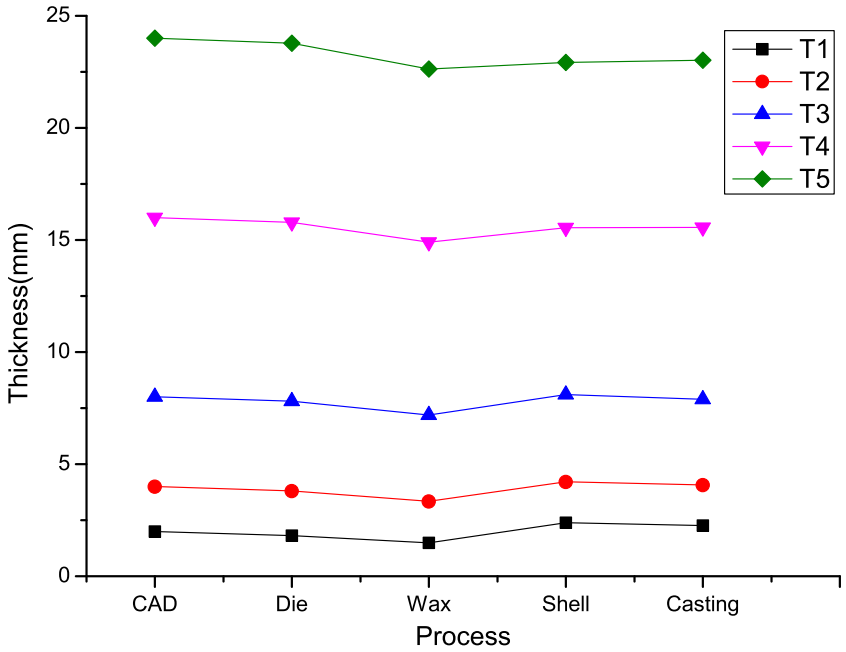

Fig. 6 Thickness changes in different processes

injection rate of 350 cm^3/s, and a nozzle diameter of 10 mm. The die and wax pattern are shown in Fig. 3a, b, respectively. The combination of process parameters in wax injection process is listed in Table 1.

2.2.2 Shell construction and material

In order to construct the shell, the slurry was prepared. The slurry for the prime coat consisted of colloidal silica binder and high temperature aluminum powder. Granular zircon formed the prime coat. The main constitution of the slurry for the backup coat was colloidal silica, ethyl silicate, fused silica, and mullite. The mullite sand was also the raw material of the stucco for the backup coat. The seal coat used no stucco. Brookfield DVII+ Pro Viscometer was used to measure the slurry viscosity. Prime coatings and backup coatings were smeared at 37–40-s viscosity on a no. 4 Zahn cup and at 27–30-s viscosity on a no. 5 Zahn cup, respectively.

Before being removed, the wax pattern was firstly completely covered by the slurry using immersion method. In order to promote an even coating, the pattern was rotated over slurry dipping pool for 120 s so that the redundant slurry can drain from different points. Then, using the rainfall method, a uniform distribution of stucco was formed. Nine backup coats, one prime coat, and one seal coat made up the shells. The pattern was dried for 24 h after the prime coat was formed. Then, the backup coats were applied and the drying time interval between backup coatings was 8 h. Finally, the seal coat was smeared and 48 h drying was applied to the pattern.

In the dewaxing process, the dewaxing pressure was 755 kPa and the dewaxing time was 25 min. Finally, the ceramic consists of 33 wt% mullite, 18 wt% Al_2O_3, 16 wt% ZrO_2, and 33 wt% SiO_2. The final ceramic shell is shown in Fig. 3c.

2.2.3 Casting and material

Before casting, the prepared ceramic shell was heated with a 1 °C/min heating rate in the electrical resistance box furnace. When the temperature raised up to 1,000 °C, the ceramic shell was moved in the casting furnace and the casting was carried on at 1,525 °C. The material used for casting was nickel-based cast superalloy. When the casting was solidified and cooled, the gating and risering system was removed. After polishing, the final casting part was constructed (as illustrated in Fig. 3d).

3 Results and discussion

3.1 Dimensional changes

In order to evaluate the changes of 3-D dimensions in every stage visually, 3-D point cloud date are compared with the CAD model via best fit alignment. Figure 4 shows that all external diameters and inner diameter relative to the original design model decrease. A large geometric dimension of the part will inevitably bring in greater shrinking. Comparing Fig. 4a, b, even the dimension changes little, we can still find that all external diameters expand and inner diameter shrinks in the dewaxing process. The comparison between Fig. 4b, c indicates that all diameters have a further shrink in the casting process and the biggest shrink is more than 5 mm.

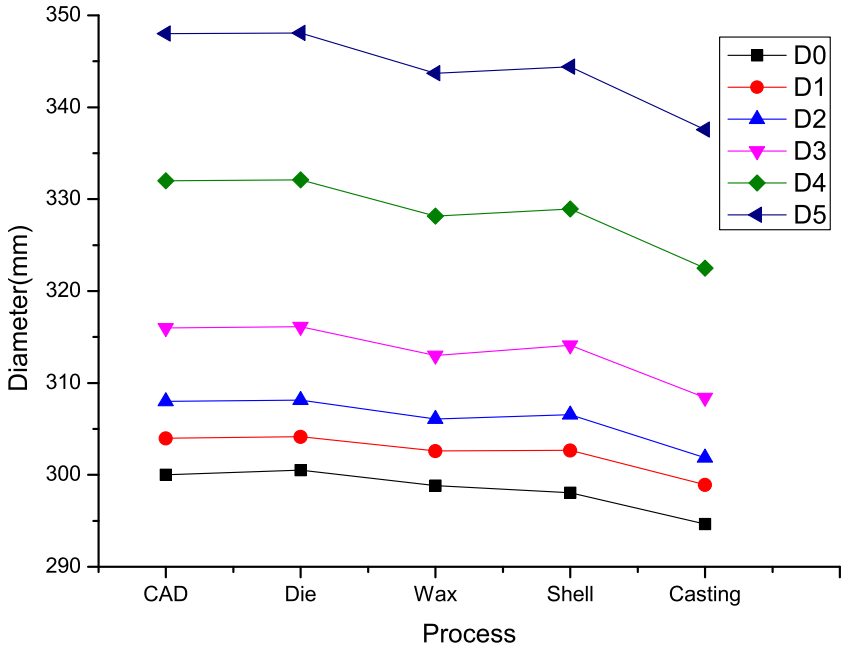

Fig. 7 Diameter changes in different processes

After cut by five cross sections in the middle of five different steps, diameters and thickness are compared to the CAD value. Figure 5 shows the changes of thickness in different processes. From Fig. 5a, c we can find that all thickness shrink and the thicker the wall is, the more the shrinking is. Figure 5b shows that the thicker walls expand, such as T1 and T2.

In order to describe the dimensional changes quantificationally, all diameters and thicknesses at different stages are extracted. Figure 6 shows that all thicknesses shrink in the wax injection process and the larger the geometric dimension, the larger the dimensional changes. The thickness T5 shrinks almost 1.5 mm. In the dewaxing process, all thicknesses expand and thinner wall expands more than their thicker counterparts. In the casting process, the thickness changes are not obvious. The thicknesses T4 and T5 of the final casting part are thinner than those of the wax. However, the thicknesses T1, T2, and T3 of the final casting part are thicker than those of the wax.

Figure 7 indicates that the diameters change a lot in the wax injection process and casting process but less in the dewaxing process. All diameters shrink in the wax injection process, and

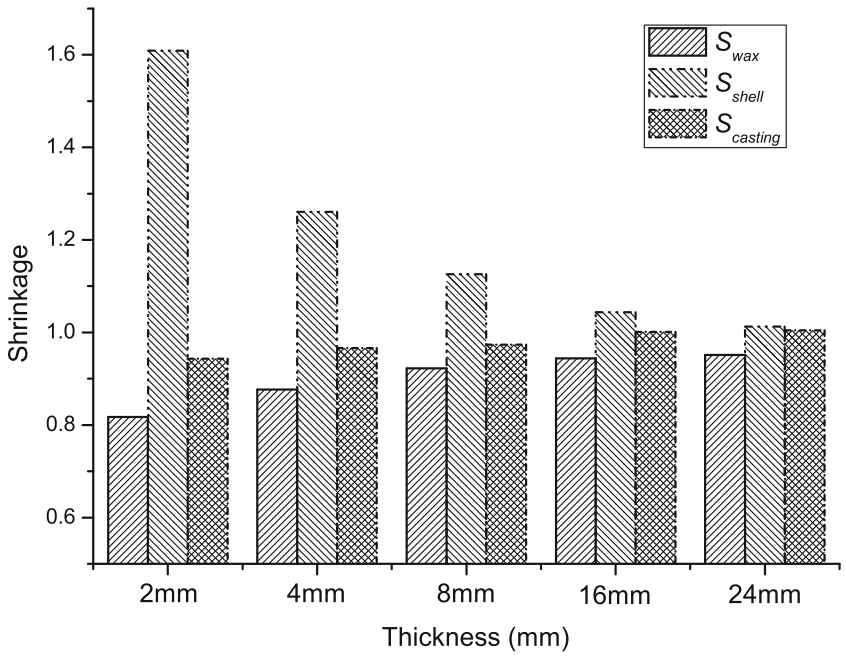

Fig. 8 The comparison of shrinkage in different processes

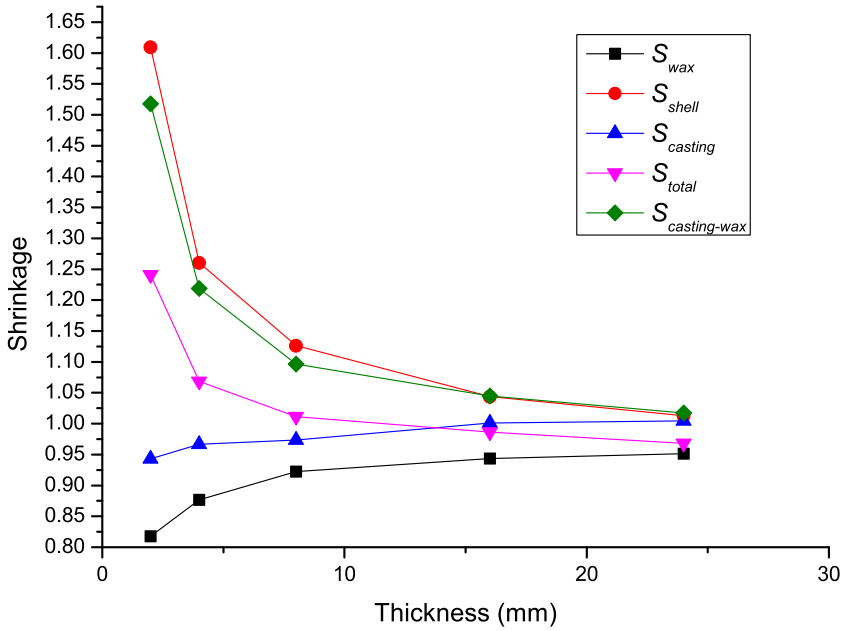

Fig. 9 Shrinkage at different thicknesses

larger diameters have larger dimensional changes. The diameter D5 shrinks more than 4 mm. This phenomenon is in accordance with that of thickness. In the dewaxing process, the external diameters (D1, D2, D3, D4, and D5) expand but the inner diameter (D0) shrinks. In the casting process, all diameters shrink and the shrinks of larger diameters are more obvious. Finally, all external diameters of the final casting part are smaller than those of the die.

3.2 Shrinkage analysis

3.2.1 Shrinkage of thickness

In order to investigate the shrinkage at different stages and the influence of thickness on shrinkage, all shrinkages of thickness in different stages are calculated according to Eqs. (1) to (5).

Figure 8 indicates that the wax and casting shrink but the shell expands at different thickness walls. The thickness shrinkage of wax is minimal that means that the shrink in the wax injection process is maximal relative to the whole ICP.

Figure 9 shows the relationship between the shrinkage and the thickness. From the shrinkage line of S_{wax} and S_{casting} in Fig. 9, we know that in the wax injection process and casting process, the shrinkages are less than 1 that means that the thicknesses shrink in these two processes. The shrinkages are smaller when the thickness is thinner that means that the dramatic shrink happened in thinner walls. In the casting process, the shrink of T5 is not obvious. The shrinkage line of S_{shell} indicates that all of thicknesses expand and the shrinkage increases when the thickness decreases in the dewaxing process. That is to say, the thinner wall expands more obviously. Figure 9 shows that the total shrinkage of T1, T2, and T3 is greater than 1, which indicates that these thicknesses expand. T4 and T5 shrink because the total shrinkage at T4 and T5 is less than 1. The shrinkage line of $S_{\text{casting-wax}}$ shows that all thicknesses of the final casting expand relative to that of wax pattern and the expansions at T1, T2, and T3 are dramatic, but those at T4 and T5 are obscure.

Table 2 Fitting results of shrinkages about the thickness

Process	Fitting curve	Parameter values	Adj. R-square
Wax injection	$S_{\text{wax}} = a - bc^{T_{\text{wax}}}$	$a = 0.94853\ b = 0.2016\ c = 0.74326$	0.99504
Dewaxing	$S_{\text{shell}} = y_0 + Ae^{-T_{\text{shell}}/t}$	$y_0 = 1.04162\ A = 1.68895\ t = 1.1684$	0.97123
Casting	$S_{\text{casting}} = a - bc^{T_{\text{casting}}}$	$a = 1.00957\ b = 0.08483\ c = 0.87807$	0.92298
Wax to casting	$S_{\text{casting-wax}} = y_0 + Ae^{-T_{\text{casting}}/t}$	$y_0 = 1.04004\ A = 1.46102\ t = 2.00307$	0.98214
Die to casting	$S_{\text{total}} = y_0 + Ae^{-T_{\text{casting}}/t}$	$y_0 = 0.98333\ A = 0.92536\ t = 1.75499$	0.97584

T_{wax}, T_{shell}, and T_{casting} are the thicknesses of wax pattern, shell, and casting part, respectively

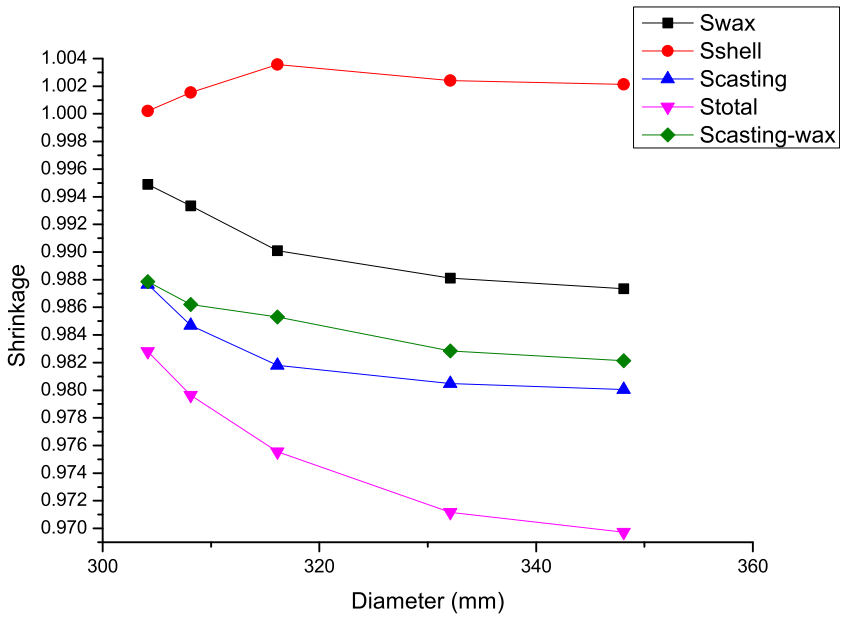

Fig. 10 Shrinkage at different diameters

In order to guide the dimensional design of the die and the reworking of the wax pattern to ensure correct dimensions and accuracy of the final casting part, all the shrinkages of the thickness in different processes are fitted by exponential function curve. The fitting formulations and fitting parameters are shown in Table 2. Table 2 shows that these fittings are reasonable and acceptable for the reason that all the Adj. R-squares of fitting curve are close to 1. $S_{\text{casting-wax}}$

3.2.2 Shrinkage of external diameter

Figure 10 shows the changes of shrinkage along with the variety of diameters in different stages. The shrinkage line of S_{shell} is above 1, and the shrinkage of diameter D3 is 1.0035, which means that all the diameters expand in the dewaxing process and the diameter D3 has the largest expansion. Other shrinkage lines are below 1 which indicates that the part shrinks in these processes. S_{wax}, S_{casting}, and S_{total} decrease with the increasing of the external diameter, and the decreasing slows down when the external diameter increases. What is more, the shrinkage lines of S_{wax} and that of S_{casting} have almost the same changes along with the variety of diameters for the reason that there are the same free shrinks in the wax injection process and casting process. Due to the irregular expansion of the shell in the dewaxing process, the variation of $S_{\text{casting-wax}}$ and that of S_{total} with the increasing of the external diameter is different from that of S_{wax} and S_{casting}. $S_{\text{casting-wax}}$ of D1 is close to S_{casting} of D1 for the shrinkage of D1 at approximately 1 in the dewaxing process.

All the shrinkages about the external diameter in different processes are also fitted by exponential function curve except the shell for its irregular. The fitting formulations and fitting parameters are shown in Table 3. Table 3 shows that all the Adj. R-squares of the fitting curve lie between 0.96712 and 0.99731, which indicates that the fittings are useful.

3.2.3 Shrinkage of inner diameter

The shrinkages of inner diameter in all processes are smaller than 1, which indicates the inner diameter shrinks in all processes (as illustrated in Fig. 11). The most dramatic shrink occurs in the casting process because the shrinkage is only

Table 3 Fitting results of shrinkage about the diameter

Process	Fitting curve	Parameter values	Adj. R-square
Wax injection	$S_{\text{wax}} = y_0 + Ae^{-D_{\text{wax}}/t}$	$y_0 = 0.98715\ A = 1.81107E9\ t = 11.56821$	0.9895
Dewaxing	–	–	–
Casting	$S_{\text{casting}} = y_0 + Ae^{-D_{\text{casting}}/t}$	$y_0 = 0.98016\ A = 4.34786E18\ t = 6.2512$	0.99731
Casting to wax	$S_{\text{casting-wax}} = y_0 + Ae^{-D_{\text{casting}}/t}$	$y_0 = 0.98148\ A = 359257.48565\ t = 16.71546$	0.96712
Casting to die	$S_{\text{total}} = y_0 + Ae^{-D_{\text{casting}}/t}$	$y_0 = 0.96915\ A = 4.63369E8\ t = 12.32395$	0.99901

D_{wax} and D_{casting} are the diameters of wax pattern and casting part, respectively. In the dewaxing process, suitable fitting curve is not found

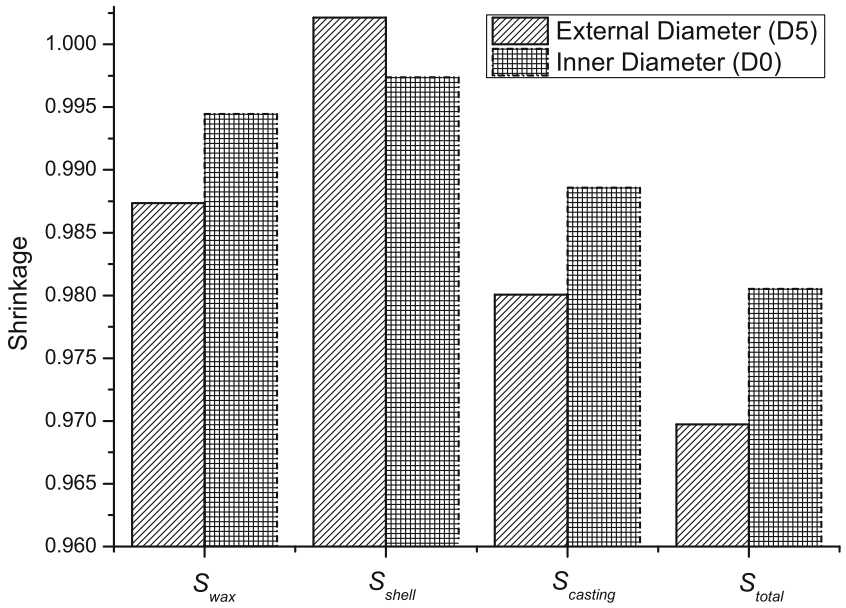

Fig. 11 The comparison of shrinkage between external diameter and inner diameter

0.9805. Figure 11 also shows the difference between the shrinkages of inner diameter and external diameter. The comparison between the shrinkages of inner diameter (D0) and that of external diameter (D5) in different processes indicates that the shrink of inner diameter is smaller than that of external diameter in the wax injection and casting process. Even though the external diameter expands and the inner diameter shrinks in the dewaxing process, the total shrinkage of inner diameter is still larger than that of external diameter for the reason that the shrinkage of external diameter is close to 1 in the dewaxing process.

3.3 Phenomenon discussion

Figure 12 is a diagrammatic sketch describing the solidification of the waxes in the die. Figure 12a indicates that the waxes at thinner wall have bigger heat transfer rate, for their surface area to volume ratio is greater. So, the thinner walls solidify more quickly than thicker walls and T1 solidifies firstly. Due to the ring and ball softening point of wax is 64.4 °C, the waxes at the thinner walls solidify quickly but liquid wax can hardly flow in to be supplement. So, low packing pressure, short holding time, low mold temperature, and melt temperature can lead to incompletable injection at thinnest walls [27]. This characteristic of the wax injection process makes the thinner walls get lower shrinkage (as the shrinkage line of S_{wax} illustrated in Fig. 9), and the greater external diameters have small shrinkage (as the shrinkage line of S_{wax} illustrated in Fig. 10). In the solidification process of the waxes in the die, the external diameters are free to shrink to their circle centers but the inner diameter (D0) is constrained by the die (as illustrated in Fig. 12b). After the wax pattern is

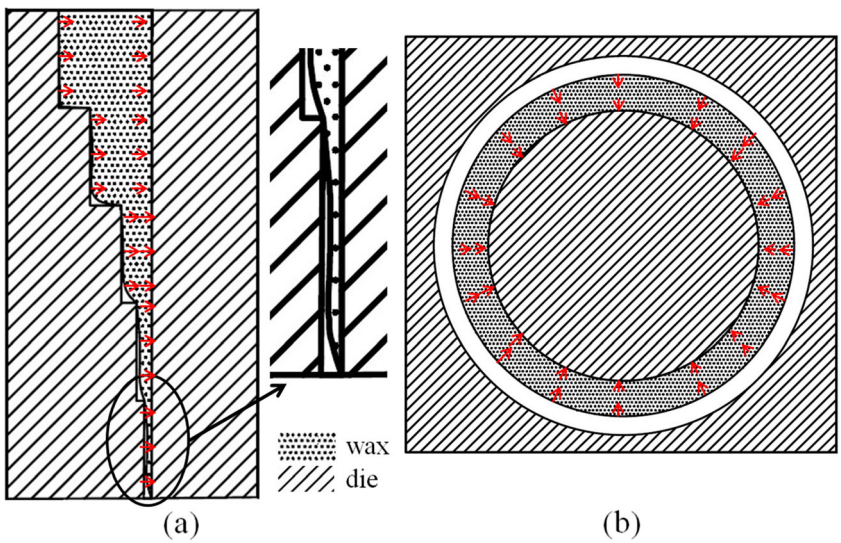

Fig. 12 The illustration of shrinkage in the wax injection process. **a** The side section view and **b** the top section view

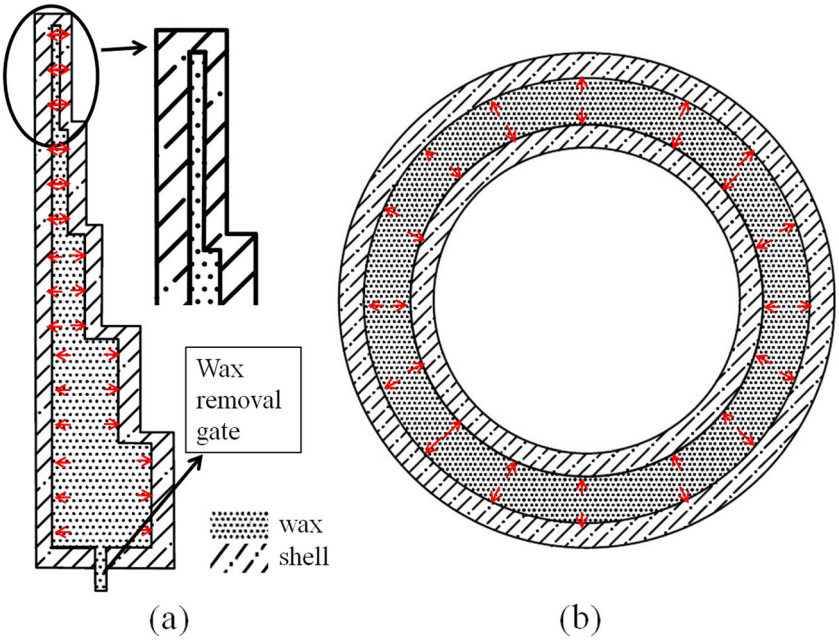

Fig. 13 The illustration of shrinkage in the dewaxing process. **a** The side section view and **b** the top section view

removed from the die, the further cooling makes the inner diameter (D0) shrink but the shrink is still constrained by four oblique supporting plates. All of these make the shrinkage greater than that of external diameters in the wax pattern construction process (as Fig. 11 illustrated).

As described by the diagrammatic sketch in Fig. 13, the waxes are melted and gasified in the dewaxing process. Figure 13a indicates that the expanding of the volume of the waxes results from a great pressure to the shell. The waxes of thinner walls are melted and gasified faster and those of the thicker walls more slowly that makes the waxes of thinner walls cannot be excreted duly. So, the thinner walls have greater pressure that leads to more dramatic expanding and greater shrinkages (as the shrinkage line of S_{shell} illustrated in Fig. 9). Extra inner pressure leads to the cracks of the shell in the dewaxing process [12, 21, 28]. Figure 13b shows that the expanding of the volume of the waxes results from a great pressure to the shell. It also makes the inner diameter shrinks to its circle center, but the external diameters expand away from their circle centers. The inner cavity thicknesses expand, so the shrinkage of D5 is more than 1 but the shrinkage of D0 is less than 1 (as illustrated in Fig. 11). However, the influence

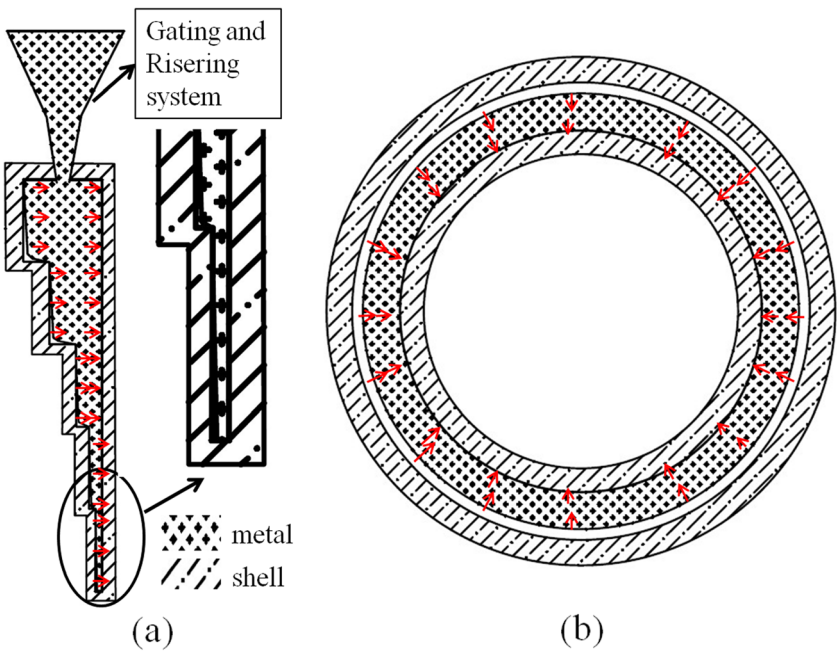

Fig. 14 The illustration of shrinkage in the casting process. **a** The side section view and **b** the top section view

of the neighboring features and the complex of the deformation of the shell make the shrinkage of the shell irregular (as the shrinkage line of S_{shell} illustrated in Fig. 10) and the shrinkage along with external diameters cannot be fitted.

As is shown in Fig. 14, the casting process has the same characteristic as that of the wax injection process. Figure 14a indicates that, for the surface area to volume ratio is greater, there are bigger heat transfer rate at thinner walls in the metal solidification process. So, the thinner walls solidify more quickly than thicker walls and T1 solidifies firstly. This characteristic of the metal solidification process also leads to the fact that the thinner walls get lower shrinkage (as the shrinkage line of $S_{casting}$ illustrated in Fig. 9) and the greater external diameters have lower shrinkage (as the shrinkage line of $S_{casting}$ illustrated in Fig. 10). However, the system of risers is added in the casting process and the liquid metal can fill in the first solidification position. That is why the shrinkage of the casting process is greater than that of wax injection process at all the thicknesses (as illustrated in Fig. 9). Figure 14b shows that the external diameters shrink freely but the inner diameter is constrained by the inner ceramic shell. It is different from the aluminum alloy die in that the deformability of the ceramic shell in high temperature [29] leads the inner diameter to shrink, but the shrink is smaller than that of external diameters. That is why the shrinkage of D5 is less than that of D0 in the casting process shown in Fig. 11. It also illustrated why all the inner diameters and external diameters shrink to their circle center, respectively, in the solidification process of the metal.

4 Conclusion

Based on the analysis of the dimensional changes and the shrinkage variation along with the different dimensions in different stages, the conclusions can be summarized as follows:

1. All the thicknesses shrink in the wax injection process, and the shrinkage of thinner wall is smaller for it solidifies firstly. In the dewaxing process, the expansion of the wax volume makes all the thicknesses expand, and in the thinner wall, the pressure is greater that leads to greater shrinkage. In the casting process, the changes of thicknesses are same to those of wax but not obvious for the system of risers is added. So, the shrinkage of T1 in the casting process is 0.9450, which is larger than that of T1 in the wax injection process. All the shrinkages in different processes, including the total shrinkage and the shrinkage from casting to wax, change (increase or decrease) exponentially along with the increase of thickness.
2. The diameters shrink a lot in the wax injection process and casting process. And, larger external diameters have smaller shrinkage for they solidify later. In this study, the shrinkage of D5 is 0.98735, which is bigger than that of D1 in the wax injection process. In the dewaxing process, all the external diameters expand but all of their shrinkages are close to 1. In other words, the expanding is small. The largest expansion is less than 0.35 %. All the shrinkages of wax injection process and casting process also change (increase or decrease) exponentially along with the increase of external diameters.
3. In the wax injection process and casting process, the shrink of inner diameter is smaller than that of external diameter because the inner diameter is constrained by the die or the shell but the external diameters are free to shrink. In the dewaxing process, the external diameters expand but the inner diameter shrinks for the expansion of the wax volume. The inner diameter shrinks in all processes, and the most dramatic shrink occurs in the casting process.

Funding This work is partially supported by the Foundation for Innovative Research Groups of the National Natural Science Foundation of China (Grant No. 51121063), National Natural Science Foundation of China (Grant No. 51175340), and National Science & Technology Pillar Program during the 12th Five-Year Plan Period (Grant No. 2012BAF06B03). The authors are grateful for these financial supports.

Appendix

Notation

a	The fitting parameter
A	The fitting parameter
b	The fitting parameter
c	The fitting parameter
D_{wax}	The diameter of wax pattern
D_{shell}	The diameter of shell
$D_{casting}$	The diameter of casting part
D0	The inner diameter
D1	The first external diameter
D2	The second external diameter
D3	The third external diameter
D4	The fourth external diameter
D5	The fifth external diameter
L_{die}	The dimensions of die
L_{wax}	The dimensions of wax pattern
L_{shell}	The dimensions of final casting part
$L_{casting}$	The dimensions of final casting part
S_{wax}	The shrinkage of wax in the wax injection process
S_{shell}	The shrinkage of shell in the dewaxing process

$S_{casting}$	The shrinkage of casting part in the casting process
$S_{casting\text{-}wax}$	The shrinkage of the final casting part relative to wax pattern
S_{total}	The shrinkage of the final casting part relative to die
t	The fitting parameter
T_{wax}	The thickness of wax pattern
T_{shell}	The thickness of shell
$T_{casting}$	The thickness of casting part
T1	The thickness of first step
T2	The thickness of second step
T3	The thickness of third step
T4	The thickness of fourth step
T5	The thickness of fifth step
y_0	The fitting parameter

References

1. Pattnaik S, Karunakar DB, Jha PK (2013) Multi-characteristic optimization of wax patterns in the investment casting process using grey–fuzzy logic. Int J Adv Manuf Technol 67(5–8):1577–1587. doi:10.1007/s00170-012-4591-4
2. Piwonka T, Wiest J (1998) Factors affecting investment casting pattern die dimensions. Incast USA 11(6):8–13
3. Wang YC, Li DY, Peng YH, Zeng XQ (2007) Numerical simulation of low pressure die casting of magnesium wheel. Int J Adv Manuf Technol 32(3–4):257–264. doi:10.1007/s00170-005-0325-1
4. Wen JL, Yang YK, Jeng MC (2009) Optimization of die casting conditions for wear properties of alloy AZ91D components using the Taguchi method and design of experiments analysis. Int J Adv Manuf Technol 41(5–6):430–439. doi:10.1007/s00170-008-1499-0
5. Ranjan R, Kumar N, Pandey R, Tiwari M (2004) Agent-based design framework for riser and gating system design for sound casting. Int J Prod Res 42(22):4827–4847. doi:10.1080/00207540410001733959
6. Thammachot N, Dulyapraphant P, Bohez ELJ (2013) Optimal gating system design for investment casting of sterling silver by computer-assisted simulation. Int J Adv Manuf Technol 67(1–4):797–810. doi:10.1007/s00170-012-4523-3
7. Gebelin JC, Jolly MR (2003) Modelling of the investment casting process. J Mater Process Technol 135(2):291–300
8. Yarlagadda PK (2000) Prediction of die casting process parameters by using an artificial neural network model for zinc alloys. Int J Prod Res 38(1):119–139
9. Yarlagadda PK, Wee LK (2006) Design, development and evaluation of 3D mold inserts using a rapid prototyping technique and powder-sintering process. Int J Prod Res 44(5):919–938. doi:10.1080/00207540500140880
10. Moorwood G, Christodoulou P, Lahnam B, Byrnes D (2000) Contraction of investment cast H13 tool steel. Int J Cast Metals 12: 457–467
11. Bonilla W, Masood SH, Iovenitti P (2001) An investigation of wax patterns for accuracy improvement in investment cast parts. Int J Adv Manuf Technol 18(5):348–356. doi:10.1007/s001700170058
12. Mishra S, Ranjana R (2010) Reverse solidification path methodology for dewaxing ceramic shells in investment casting process. Mater Manuf Process 25(12):1385–1388
13. Hock T, Trevor S, Christodoulou P, Yarlagadda P (2003) Experimental studies on the accuracy of wax patterns used in investment casting. Proc IME B J Eng Manufact 217(2):285–289
14. Rahmati S, Akbari J, Barati E (2007) Dimensional accuracy analysis of wax patterns created by RTV silicone rubber molding using the Taguchi approach. Rapid Prototyp J 13(2):115–122. doi:10.1108/13552540710736803
15. Morrell R, Quested PN, Jones S, Ford DA (2006) Dimensional stability of ceramic casting moulds. National Physical Laboratory
16. Jiang J, Liu XY (2007) Dimensional variations of castings and moulds in the ceramic mould casting process. J Mater Process Technol 189(1):247–255
17. Jiang W, Fan Z, Liao D, Dong X, Zhao Z (2010) A new shell casting process based on expendable pattern with vacuum and low-pressure casting for aluminum and magnesium alloys. Int J Adv Manuf Technol 51(1–4):25–34. doi:10.1007/s00170-010-2596-4
18. Sabau A (2005) Numerical simulation of the investment casting process. Transactions of Trans Am Foundry Soc 113:407–417.
19. Sabau AS (2006) Alloy shrinkage factors for the investment casting process. Metall Mater Trans B 37(1):131–140
20. Sabau AS, Porter WD (2008) Alloy shrinkage factors for the investment casting of 17-4PH stainless steel parts. Metall Mater Trans B 39(2):317–330
21. Chen X, Li D, Wu H, Tang Y, Zhao L (2011) Analysis of ceramic shell cracking in stereolithography-based rapid casting of turbine blade. Int J Adv Manuf Technol 55(5–8):447–455. doi:10.1007/s00170-010-3064-x
22. Zhang DH, Jiang RS, Li JL, Wang WH, Bu K (2010) Cavity optimization for investment casting die of turbine blade based on reverse engineering. Int J Adv Manuf Technol 48(9–12):839–846
23. Wu H, Li D, Chen X, Sun B, Xu D (2010) Rapid casting of turbine blades with abnormal film cooling holes using integral ceramic casting molds. Int J Adv Manuf Technol 50(1–4):13–19. doi:10.1007/s00170-009-2502-0
24. Dong Y, Zhang D, Bu K, Dou Y, Wang W (2011) Geometric parameter-based optimization of the die profile for the investment casting of aerofoil-shaped turbine blades. Int J Adv Manuf Technol 57(9–12):1245–1258. doi:10.1007/s00170-011-3681-z
25. Fu Z, Mo J (2010) Multiple-step incremental air-bending forming of high-strength sheet metal based on simulation analysis. Mater Manuf Process 25(8):808–816
26. Martínez S, Cuesta E, Barreiro J, Álvarez B (2010) Analysis of laser scanning and strategies for dimensional and geometrical control. Int J Adv Manuf Technol 46(5–8):621–629
27. Tsoukalas V (2008) Optimization of injection conditions for a thin-walled die-cast part using a genetic algorithm method. Proc IME B J Eng Manufact 222(9):1097–1106
28. Everhart W, Lekakh S, Richards V, Smith J, Li H, Chandrashekhara K, Nam HZP (2012) Foam pattern aging and its effect on crack formation in investment casting ceramic shells Trans Am Foundry Soc 120:237–244.
29. Song Y, Yan Y, Zhang R, Lu Q, Xu D (2002) Boundary model between casting and mould and its influence on the dimensional accuracy analysis of precision castings. Proc IME B J Eng Manufact 216(8):1123–1134